

Learning ORDER-Aware Multimodal Representations for Composite Materials Design

Xinyao Li, Hangwei Qian, Jingjing Li, Ivor Tsang

Abstract—Artificial intelligence (AI) has shown remarkable success in materials discovery and property prediction, particularly for crystalline and polymer systems where material properties and structures are dominated by discrete graph representations. Such graph-central paradigm breaks down on composite materials, which possess continuous and nonlinear design spaces that lack well-defined graph structures. General composite descriptors, e.g., fiber volume and misalignment angle, cannot fully capture the fiber distributions that fundamentally determine microstructural characteristics, necessitating the integration of heterogeneous data sources through multimodal learning. Existing alignment-oriented multimodal frameworks have proven effective on abundant crystal or polymer data under discrete, unique graph-property mapping assumptions, but fail to address the highly continuous composite design space under extreme data scarcity. In this work, we introduce ORDinal-aware imagE-tabulaR alignment (ORDER), a multimodal pretraining framework that establishes **ordinality** as a core principle for composite material representations. ORDER ensures that materials with similar target properties occupy nearby regions in the latent space, which effectively preserves the continuous nature of composite properties and enables meaningful interpolation between sparsely observed designs. We evaluate ORDER on a public Nanofiber-enforced composite dataset and an internally curated dataset that simulates the construction of carbon fiber T700 with diverse fiber distributions. ORDER achieves consistent improvements over state-of-the-art multimodal baselines across property prediction, cross-modal retrieval, and microstructure generation tasks. Our work demonstrates learning semantically continuous multimodal features are fundamental for composite materials, and provides a reliable pathway toward data-efficient universal multimodal intelligent systems.



1 INTRODUCTION

Materials science forms the foundation for technological innovation across diverse fields, from semiconductors and catalysis to energy storage and biomedicine [1]. Historically, materials discovery has relied on heuristic experimentation, theory, or computational approaches [2], [3]. While foundational, these methods remain labor-intensive and time-consuming [4], [5], requiring years to progress from discovery to deployment. Recent advances in machine learning, especially deep learning, have inspired data-driven techniques in materials science [6], [7], substantially accelerating the research process [8]. These methods extract vast knowledge and patterns from large-scale materials databases. They primarily operate on string descriptors or graph structures to encode key information such as chemical compositions, crystal parameters, processing conditions, and have demonstrated remarkable effectiveness in tasks including property prediction [9], [10], materials design [11], and structure-application mapping [12]. While recent characterization techniques generate diverse data modalities, such as microscopy images revealing microstructural features [13] and X-ray diffraction patterns providing crystallographic information [14], they typically serve as complementary verification or alternative representations of information already encoded in material graph structures. For widely-researched materials like crystals and polymers, their graph

representations sufficiently reflect material structure and properties in most applications [15], [16].

However, this landscape changes for composite materials. Unlike crystals or polymers, composite properties are determined by the continuous, nonlinear, and infinitely variable fiber distributions within the polymer matrix, which discrete graph-based representations cannot encode. General tabular descriptors for composites (e.g., fiber volume fraction and mean misalignment angle) constrain only high-level material compositions but fail to capture the spatial fiber distributions. Furthermore, the nonlinear property-structure relationships result in dramatic property changes triggered by minor changes in fiber arrangements [17]. Therefore, the fiber spatial distributions reflected in microscopy images become essential for composite materials, motivating us to unify coarse compositional control (in tabular descriptors) with actual fiber distributions (microstructural images) using multimodal pretraining techniques, such as Contrastive Language-Image Pretraining (CLIP) [18]. CLIP establishes a shared latent space where paired features (such as images and texts) from the same sample are drawn together while unpaired ones are pushed apart. This alignment framework has been extended to various modalities including tabular data [19], [20], videos [21], and audio [22]. It has also been proven effective in material science: MultiMat [10] constructs a unified latent space for crystalline with modalities including density of states, charge density, and text descriptions, enabling materials property prediction and discovery. Khan *et al.* [12] leverage powder X-ray diffraction patterns, chemical precursors, and crystal graphs to create synthesis-to-application maps for metal-organic frameworks. Huang *et al.* [9] develop a

- Work done during Xinyao Li's internship at A*STAR CFAR, Singapore.
 - Xinyao Li, Jingjing Li are with University of Electronic Science and Technology of China, Chengdu 610054, China.
 - Hangwei Qian, Ivor Tsang are with A*STAR CFAR, Singapore.
- Manuscript received; revised.

multimodal dataset encompassing chemical precursors, 2D graphs, 3D geometries, fingerprints, and textual descriptions for polymer materials.

These approaches demonstrate strong performance on abundant crystal and polymer data, whose multimodal representation pairs, e.g., graph structures and target properties, are typically discrete and uniquely associated. However, these conditions break down for composite materials, where fiber distribution, orientation, and density vary continuously within the design space. Moreover, the extreme data scarcity in composite materials poses a critical challenge: with limited multimodal samples (generally hundreds) representing less than 0.001% of possible configurations, how to enable reliable materials design and understand across unobserved regions of this vast design space? Current multimodal methods for material science [10], [12], [23] treats materials as discrete entities to be matched across modalities, which lack the ability to interpolate between sparse samples or preserve the property continuity essential for inverse design.

In this work, we argue that *ordinality* should serve as a core organizing principle for multimodal learning in composite materials. We propose ORDinal-aware image-tabular alignment (ORDER), a multimodal pretraining framework that constructs a latent space reflecting both cross-modal alignment and ordinal property characteristics. Beyond learning correspondence between tabular descriptors and microstructural images, ORDER ensures that materials with similar target properties are embedded in nearby regions, thereby preserving the semantic continuity of composite design spaces and enable effective learning from sparse observations. Our key design to achieve this is ordinal-aware contrastive learning within each modality, which draws closer samples with similar target properties. To optimize against current multimodal contrastive learning process that equally separates any mismatch pair while not disturbing its cross-modal alignment effect, one straightforward solution is to weight the two objectives appropriately but requires grid-search on validation data. To achieve adaptive and dynamic weighting on any dataset, we further introduce preference-guided multitask learning [24] to ensure Pareto optimal of the bi-objective optimization process. In accordance with prior work [23], we focus on aligning tabular and visual modalities, as descriptor and property information is typically documented in tabular form while microscopy images provide complementary microstructural details. While existing approaches usually resort to training smaller neural networks [25] due to the limited multimodal composite datasets, we instead propose to adapt the vision transformer [26] from the pretrained CLIP model [18] using parameter-efficient fine-tuning (PEFT) [27].

We evaluate ORDER on two real-world multimodal composite datasets: the public Nanofiber-enforced composite dataset from [23], and our in-house multimodal dataset on carbon fiber T700 (CF-T700): a high-strength, intermediate-grade material known for its excellent balance of stiffness, power, and durability. We exploit the vast design space and obtain corresponding target properties and microstructure images to form this first multimodal dataset for CF-T700. Experimental results show that ORDER not only achieves superior retrieval accuracy but also retrieves

physically meaningful candidates. The aligned and ordinal multimodal representations proven to be universally effective for target property prediction and generative modeling tasks. We show that ORDER addresses the challenge of learning the infinite continuous design space under extreme data scarcity, providing both a practical framework and fundamental insight for composite materials.

2 RESULTS

2.1 Construction of Composite dataset

We propose the multimodal CFRP dataset (referred to as the Composite data for the rest of the paper) to enable the construction of vision-tabular models. CFRP is a composite material made of a polymer matrix (e.g., epoxy) and carbon fibers (as reinforcement). Specifically, we focus on the varying random unidirectional carbon fibers in epoxy matrix of the CF-T700 material. We alter the volume fraction (Vf) in the composite and explore different mean misalignment angle (MMA) of the fibers as descriptors. Based on the Representative Volume Element (RVE) [28] method from the Ansys Material Designer software, we simulate the corresponding microstructures and target properties (tensile yield strength, elongation) of the input descriptors. We modeled 436 different descriptor combinations with Vf ranging from 0.32 to 0.65 and MMA ranging from 0 to 5 degrees, and obtain their corresponding tabular-image pairs for our Composite dataset. More details are in Section 4.1.

2.2 Ordinal-aware image-tabular alignment

We present ORDER (ORDinal-aware image-tabular alignment), a multimodal pretraining framework that not only captures cross-modal relationships but also preserves property ordinality inherent in composite material data. Figure 1 illustrates the representation learning stage of ORDER and diverse downstream applications based on the pretrained multimodal representations.

The pretraining procedure operates on the Composite datasets described in Section 2.1, as well as a public Nanofiber dataset [23]. The inputs include descriptors in tabular form and corresponding microstructural images. Denote the i_{th} input vision microstructure as v_i , and its corresponding table feature (descriptor in tabular form) as t_i . In the second step of Figure 1a, ORDER introduces a vision encoder E_v and table encoder E_t to process the original image and tabular inputs, respectively, and map them to a shared latent feature space: $h_i^t = E_t(t_i)$, $h_i^v = E_v(v_i)$, where $h_i^t, h_i^v \in \mathbb{R}^d$ are d -dimension features of tabular and vision modality, respectively.

ORDER pursues two complementary objectives. First, *cross-modal alignment* ensures that feature similarity between matched image-tabular pairs is higher than that of mismatched pairs: $\text{sim}(h_i^t, h_i^v) > \text{sim}(h_i^t, h_j^v)$ for all $i \neq j \in [1, N]$, where N denotes the dataset size. Following established multimodal learning approaches [18], we employ cross-modal contrastive loss $\mathcal{L}_{\text{align}}$ to achieve this alignment (upper panel of Figure 1a, stage 3). This objective pulls closer features from corresponding image-tabular pairs while pushing away mismatched cross-modal pairs and same-modality pairs. However, as illustrated in

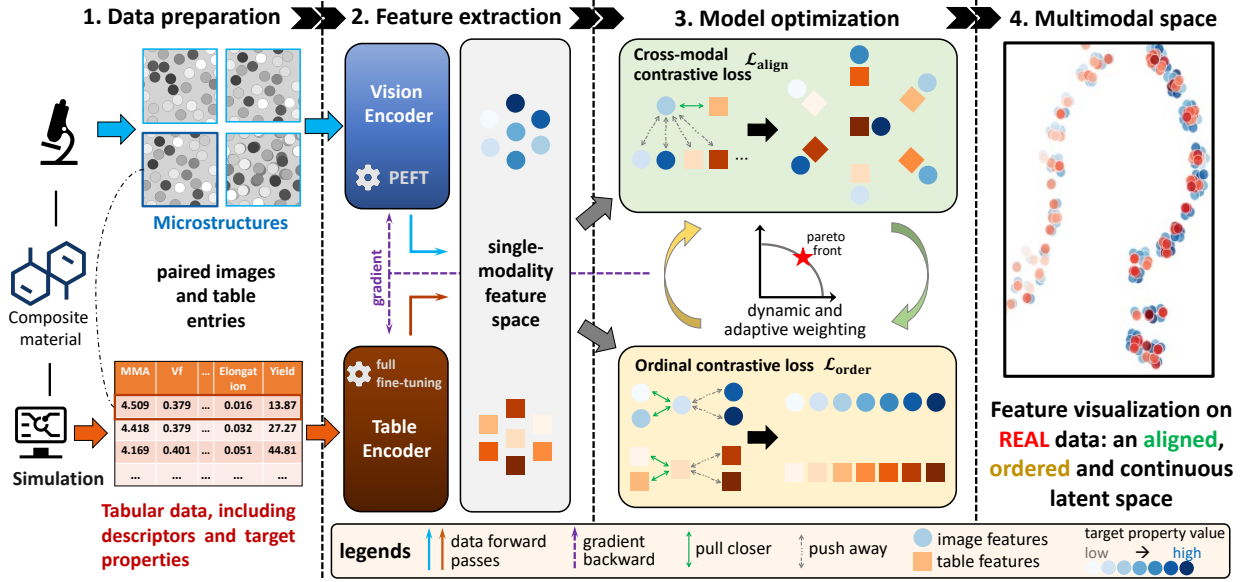
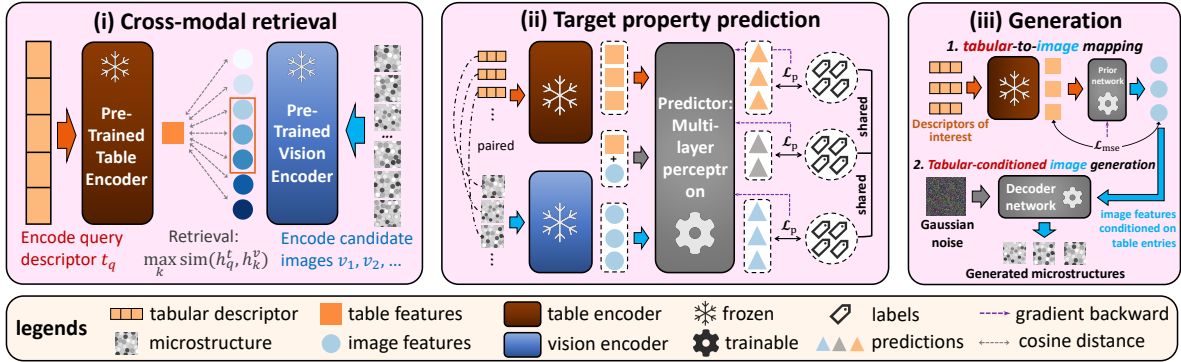
a Image-tabular representation learning**b** Downstream applications based on the multimodal space

Fig. 1. **a** The pretraining pipeline of ORDER. Step 1, raw composite data images and target properties are obtained by simulating on various descriptors, and organized as pairs. Step 2, paired tabular descriptors and microstructure images are encoded into a shared latent space via dedicated encoders. Step 3, we apply cross-modal contrastive learning *between* modalities to enforce image-tabular alignment, and ordinal-aware contrastive learning *within* each modality to produce property-ordered embeddings. Preference-guided multitask optimization addresses potential conflicts during the bi-objective optimization. Step 4, the training process yields an aligned and ordinal-aware multimodal latent space. **b** Downstream tasks. The pretrained features are then frozen and serve as the initial starting point for various downstream tasks: (i) Cross-modal retrieval by finding the most similar candidate features with the query feature. The ordinal awareness encoded in features ensures physically meaningful candidates. (ii) Property prediction by training lightweight prediction heads based on the pre-aligned features. (iii) Descriptor-conditioned microstructure generation from tabular inputs. Based on the pretrained feature space, a prior network is trained to translate tabular features into image features and a decoder network learns to reverse them into images.

stage 3 of Figure 1a, the standard alignment loss treats all negative pairs equally and ignores the continuous and ordinal characteristics of material property values. Consequently, the resulting feature space may position materials with distinct properties in near regions, potentially confusing downstream tasks. To address this limitation, ORDER’s second objective enforces *ordinal awareness* in the learned representations. Inspired by Zha *et al.* [29], we apply contrastive loss \mathcal{L}_{order} within each modality to ensure that samples with similar target properties are embedded closer in the feature space. As depicted in the lower panel of Figure 1a (stage 3), this objective produces a continuous and ordered feature distribution aligned with property values.

By combining cross-modal alignment and ordinal-aware objectives, ORDER constructs a multimodal latent space that is both semantically aligned and property-ordered. But optimizing these dual objectives can introduce conflicting gradients; to be more specific, cross-modal alignment loss

may push apart image features of materials with similar properties, while ordinal-aware loss draws them together. We propose two strategies to mitigate these conflicts: (1) ORDER- α weights the two objectives with a fixed hyperparameter α determined via grid search, and (2) ORDER-dyn dynamically adjust the weights on the losses during training with preference-guided multitask learning [24]. In our experiments, we empirically show that ORDER- α achieves better performance on certain tasks with grid search, while the hyperparameter-free ORDER-dyn exhibits robust performance across diverse downstream tasks. The scarcity of fully annotated multimodal materials datasets has led previous approaches to initialize vision encoders with unimodal models such as ResNet50 [25], constraining model capacity. ORDER instead adopts the pretrained Vision Transformer [26] from CLIP [18], a large-scale vision-language foundation model. We demonstrate that parameter-efficient fine-tuning (PEFT) [27] enables effective knowledge trans-

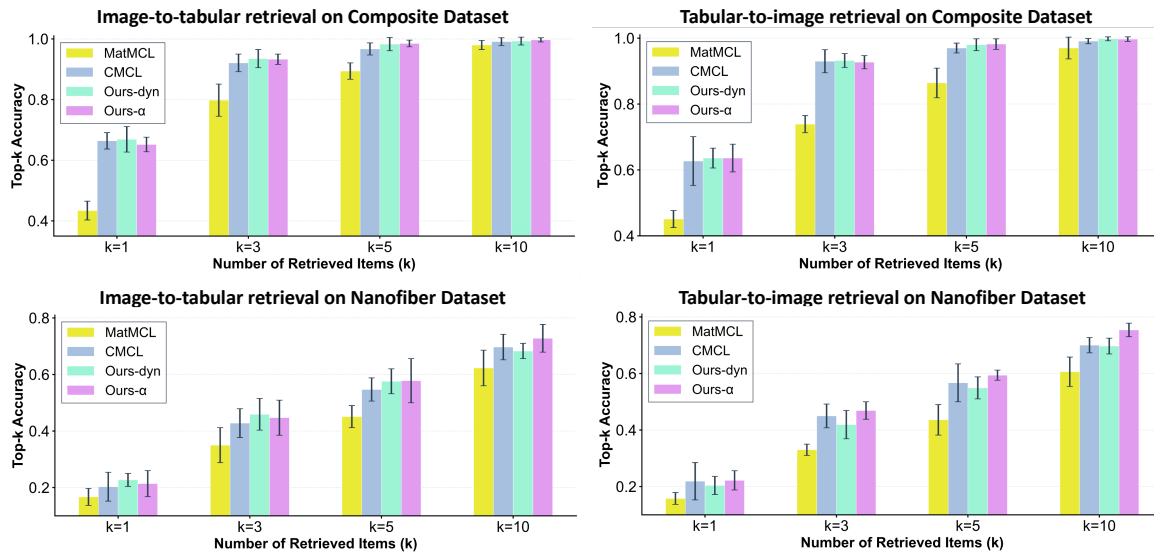
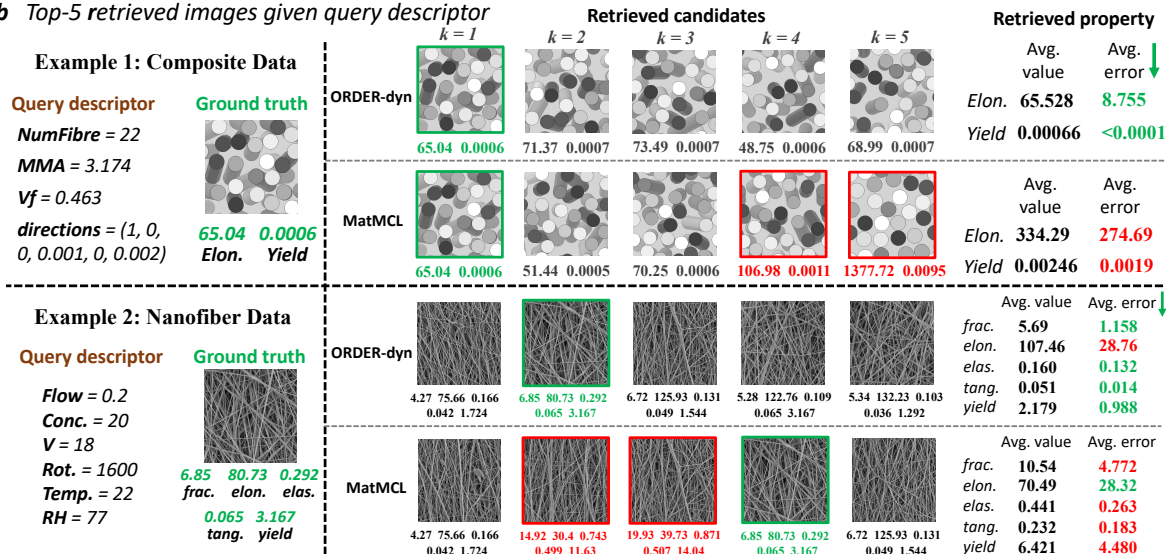
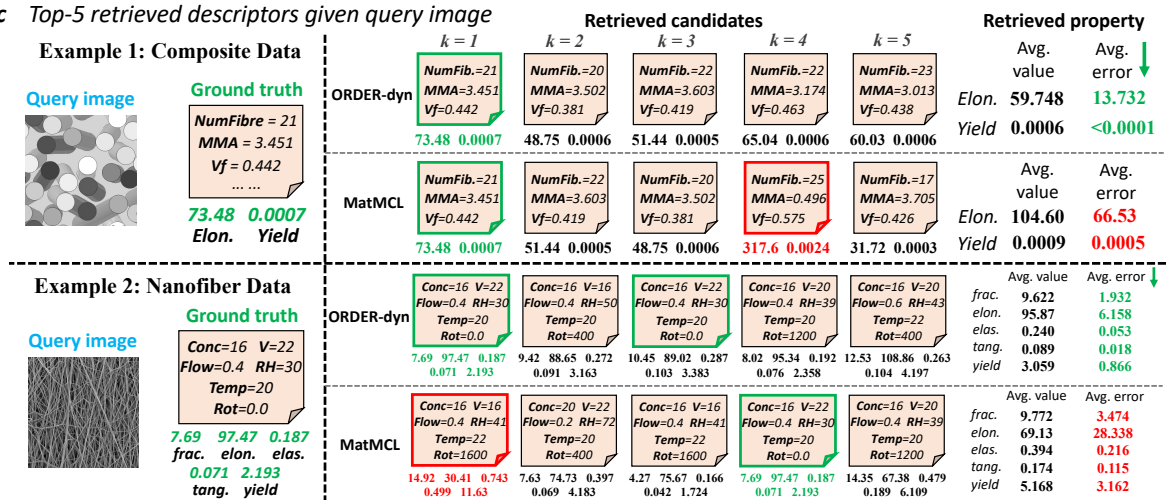
a Top- k cross-modal retrieval accuracy**b** Top-5 retrieved images given query descriptor**c** Top-5 retrieved descriptors given query image

Fig. 2. **a** Cross-modal retrieval results w.r.t. accuracy with varying number of retrieved candidates (k). ORDER variants consistently outperform vanilla cross-modal contrastive learning (CMCL) and MatMCL. **b** Examples on top-5 retrieved images given tabular descriptors. The left panel shows query descriptors and the corresponding ground-truth image. The middle panel shows top-5 retrieved examples, with their target property values displayed beneath each retrieved item. Samples with green borders represent correct retrievals (ground truth), while red borders indicate unwanted candidates with substantially different target properties. The right panel presents statistics of the properties of retrieved samples. ORDER achieves markedly lower property deviation errors across retrieved candidates. **c** Examples on top-5 retrieved descriptors given a query image.

TABLE 1

Root mean square error (RMSE) of prediction tasks on Composite and Nanofiber datasets using pretrained tabular and image features. Each column refers to one target property to forecast. Best results for each property are bolded.

Tabular features								Image features							
Method	frac.	elon.	Nanofiber		Composite			Method	frac.	elon.	Nanofiber		Composite		
			elastic	tangent	yield	Yield	Elon.				elastic	tangent	yield	Yield	Elon.
<i>Modality-specific baselines</i>															
TabPFN	3.134	17.852	0.086	0.093	2.546	209.755	0.0018	ResNet50	2.665	23.932	0.099	0.101	2.427	227.339	0.0020
XGBoost	2.993	17.474	0.094	0.104	2.537	205.301	0.0019	ViT-B/16	2.653	23.570	0.095	0.096	2.333	231.743	0.0020
CatBoost	3.105	16.036	0.094	0.102	2.568	200.671	0.0017	ResNet101	2.686	24.135	0.103	0.104	2.466	203.963	0.0016
LightGBM	3.077	18.663	0.099	0.113	2.697	204.357	0.0021	ViT-B/32	2.729	23.447	0.101	0.103	2.478	211.346	0.0016
<i>Multimodal pretraining - ViT-B/16</i>															
MatMCL	2.912	20.244	0.086	0.100	2.359	235.361	0.0018	MatMCL	2.625	24.096	0.096	0.095	2.240	255.027	0.0021
CMCL	2.632	20.376	0.086	0.097	2.240	234.221	0.0019	CMCL	2.560	24.982	0.094	0.095	2.267	232.319	0.0019
Ours-dyn	1.992	14.814	0.061	0.069	1.542	194.615	0.0017	Ours-dyn	2.210	23.348	0.082	0.080	1.888	189.706	0.0017
Ours- α	1.702	11.992	0.061	0.072	1.785	194.936	0.0016	Ours- α	2.155	22.118	0.086	0.076	1.962	140.205	0.0011
<i>Multimodal pretraining - ViT-B/32</i>															
MatMCL	2.870	19.618	0.094	0.101	2.384	225.647	0.0018	MatMCL	2.773	24.267	0.097	0.100	2.408	262.969	0.0021
CMCL	2.875	21.658	0.096	0.106	2.483	229.282	0.0018	CMCL	2.691	25.441	0.101	0.102	2.452	229.407	0.0019
Ours-dyn	1.977	14.600	0.070	0.068	1.513	196.793	0.0017	Ours-dyn	2.309	23.276	0.089	0.087	1.977	185.248	0.0016
Ours- α	1.795	11.437	0.065	0.063	1.731	195.462	0.0017	Ours- α	2.177	22.811	0.084	0.079	1.923	139.532	0.0011

fer: the rich pretrained representations in CLIP are preserved while domain-specific materials knowledge is injected using only hundreds of paired samples. For the tabular encoder, we employ FT-Transformer [30] following previous work [23]. Both encoders are frozen after pretraining and the learned multimodal representations are applied to downstream tasks (Figure 1b). Detailed pretraining process can be found in Section 4.3.

We evaluate ORDER’s representation quality on our Composite dataset and the public Nanofiber dataset, through diverse downstream tasks including cross-modal retrieval, property prediction, and microstructure generation. The following sections present comprehensive experimental results across these tasks.

2.3 Cross-modal retrieval results

Cross-modal retrieval aims to identify the most relevant counterpart in one modality given a query in a different modality, which is fundamental to multimodal materials informatics and inverse design. Without additional fine-tuning, the cosine similarities between ORDER-pretrained features can be computed, as illustrated in Figure 1b(i) and detailed in Section 4.4.1. We benchmark ORDER-dyn and ORDER- α (denoted as Ours-dyn and Ours- α in figures) against two baselines: (1) vanilla Cross-Modal Contrastive Learning (CMCL) with PEFT, and (2) MatMCL [23], a state-of-the-art image-tabular pretraining framework for material data. All methods employ identical vision and tabular backbones (ViT-B/16) to ensure fair comparison. Results are presented in Figure 2.

Figure 2a presents quantitative Top- k retrieval performance, where k denotes the number of retrieved candidates. Retrieval is deemed successful if the the correct corresponding counterpart is included in appears among the k candidates. Both ORDER variants and CMCL substantially outperform MatMCL across all tasks, demonstrating that PEFT effectively transfers domain-specific materials knowledge into foundation models while preserving their pretrained capabilities. ORDER- α achieves optimal performance in most cases through our proposed two variants. ORDER-dyn attains comparable accuracy to CMCL using dynamically adapted weights. Notably, incorporating intra-

modal ordinal-aware contrastive loss may introduce conflicted gradients during cross-modal alignment, potentially limiting raw retrieval accuracy gains. However, this tradeoff is intentional. Our primary objective is not just maximizing Top- k accuracy, but rather constructing a physically meaningful feature space. We therefore assess representation quality through downstream task performance and the physical soundness of retrieved candidates. In practical inverse design scenarios, researchers and practitioners seek to identify multiple candidates with target properties similar to a query sample for subsequent experimental validation. Standard Top- k accuracy metrics only verify ground-truth inclusion but disregard the quality of remaining candidates, which limits its practicability in material applications.

To address the limitation of the current Top- k metric, we analyze the target property distributions of all retrieved items to evaluate their overall quality (Figure 2b,c). We examine material properties such as yield strength and elongation, which dictate material characteristics and fidelity. Green-bordered samples indicate ground-truth matches, while red-bordered samples deviate substantially from the query. We can observe that, by the definition of Top- k retrieval accuracy ($k = 5$ in our case), *all* examples are ‘correct’ retrievals since they include the ground truth. However, the quality of non-ground-truth candidates differs dramatically between ORDER and MatMCL. MatMCL frequently retrieves candidates with target properties deviating from the query sample. We show that the average property difference between ground truth and all retrieved items is considerably higher for MatMCL than for ORDER. This discrepancy arises because MatMCL enforces only cross-modal alignment, treating all negative samples equivalently regardless of their ordinal properties. In contrast, ORDER’s ordinal-aware objective ensures that materials with similar target properties cluster together in the feature space, yielding retrieval sets where all candidates exhibit relevant property values. The above limitations are also observable in CMCL, suggesting the need of explicit ordinal constraints.

2.4 Property prediction performances

Accurately predicting target material characteristics from input features is one of the essential tasks in materials

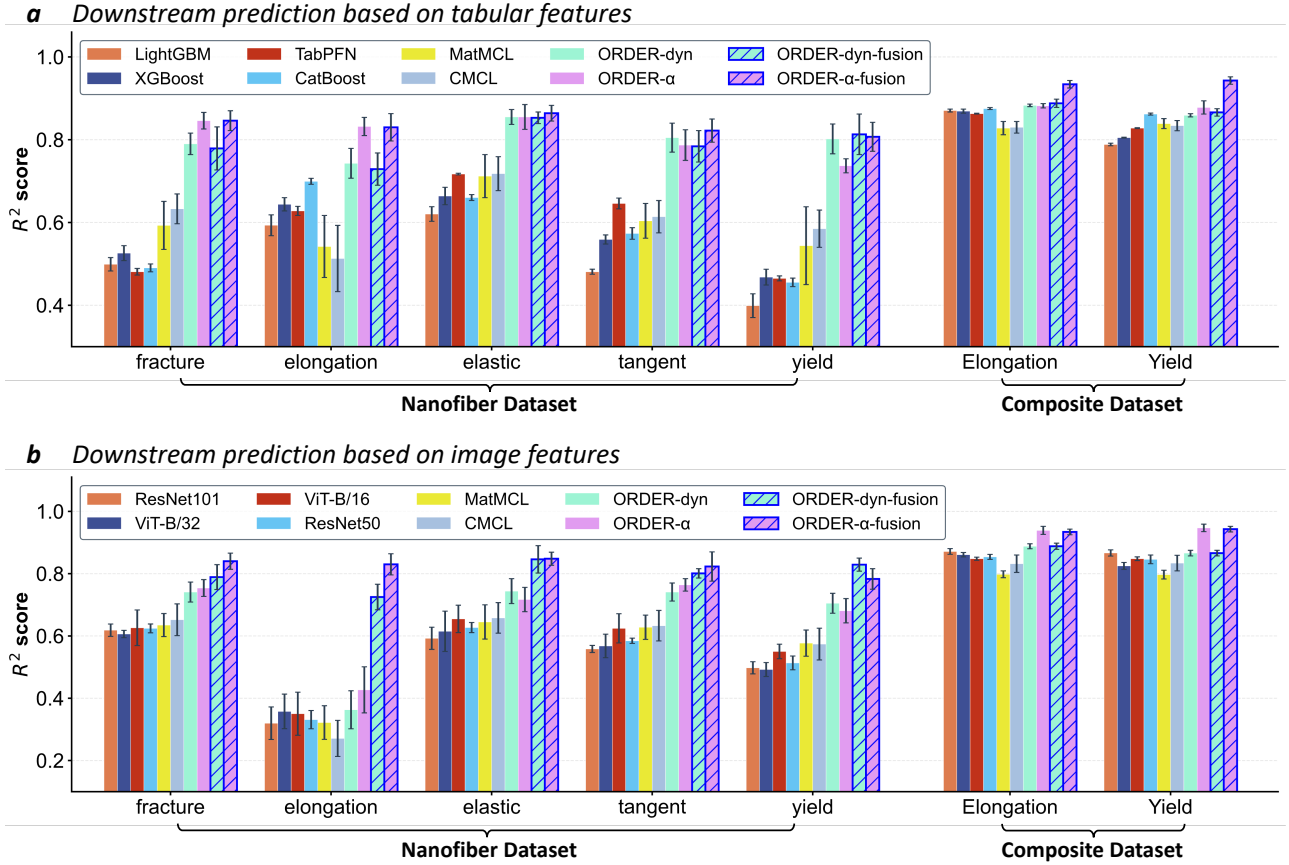


Fig. 3. Target property prediction performance on Composite and Nanofiber datasets. For multimodal pretraining methods (ORDER, MatMCL, CMCL), extracted features are frozen and used to train an MLP for property prediction. All multimodal pretraining methods use ViT-B/16 as backbone. ORDER achieves substantial improvements on both datasets compared with multimodal and modality-specific baselines. The modality-fusion results (highlighted with borders and shadows) bring even better performances by incorporating both modality strengths.

science, as it enables materials design by bypassing costly experimental characterization. This task typically operates on tabular data, where established tabular-specific methods such as XGBoost [31], TabPFN [32], CatBoost [33] and LightGBM [34] have demonstrated strong performance. As ORDER is a multimodal framework involving image and tabular modalities, we additionally evaluate vision-based prediction capabilities by comparing against general vision models including ImageNet-pretrained ResNet50, ResNet101 [25] and Vision Transformer (ViT-B/16, ViT-B/32) [26]. For modality-specific baselines, we train or fine-tune models directly on raw inputs (t_i, v_i). For multimodal pretraining methods (ORDER, MatMCL, CMCL), encoders remain frozen after pretraining, and pre-extracted features (h_i^t, h_i^v) are used to train a lightweight multilayer perceptron (MLP) for property prediction. We evaluate all methods on predicting fracture strength, elongation, elastic modulus, tangent modulus, and yield strength for the Nanofiber dataset, and yield strength and elongation for the Composite dataset. All experiments are repeated five times independently with mean values reported. Results are presented in Table 1 (RMSE) and Figure 3 (R^2 scores).

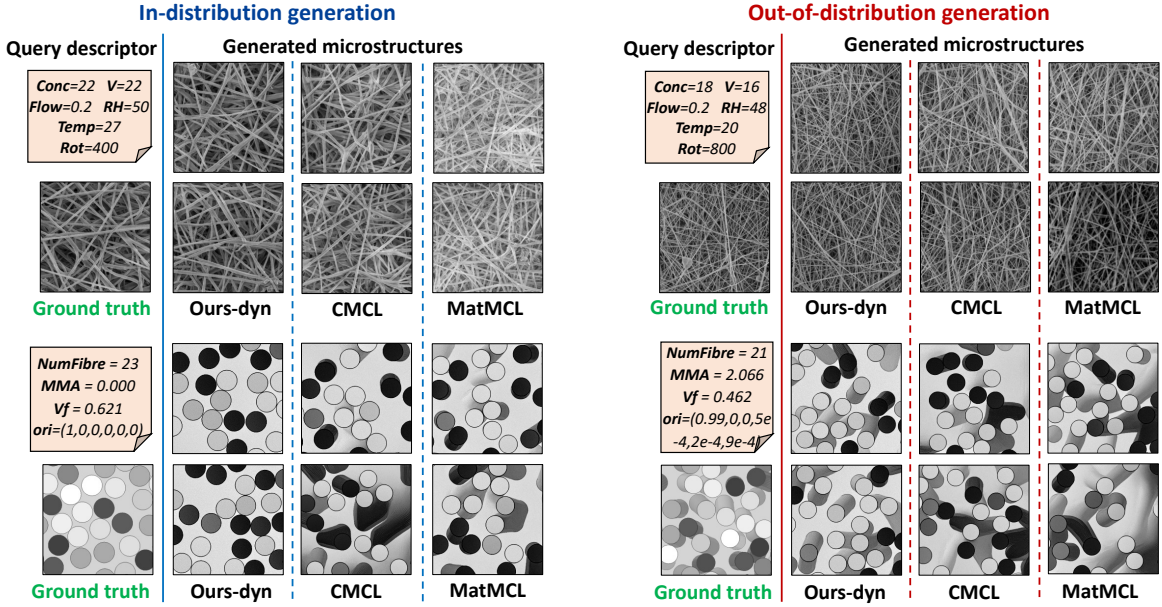
ORDER achieves the lowest prediction error across all target properties. For *tabular-based prediction*, specialized tabular methods such as CatBoost perform competitively on the simpler Composite dataset but struggle with the more complex Nanofiber data, where our ORDER- α re-

duces prediction error by 30.2% on average compared to CatBoost. ORDER-dyn and ORDER- α exhibit comparable performance on Nanofiber, with ORDER- α showing modest advantages on Composite data. For *image-based prediction*, ORDER- α achieves substantially lower errors than all baselines on Composite data, reducing error by more than 40% compared to MatMCL and CMCL.

We observe that prediction performances based on different modalities (tabular descriptors versus images) differ across target properties and datasets. This pattern complies with our claim that descriptors and microstructure images are both essential for composite materials. On our Composite dataset with clear microstructures and coarse-level descriptors (only include fiber density and misaligned angle), image-based predictions are more comprehensive. Nanofiber dataset includes more descriptive descriptors (detailed in [23]), making tabular-based prediction superior for some properties more related to descriptors (e.g., elongation). Therefore, our introduction of multimodal information for composite material is necessary and effective. Table 1 also includes comparisons on different backbones (ViT-B/16 and ViT-B/32). Our methods consistently surpass the multimodal baselines on all backbones. The two backbones exhibit comparable performance across all tasks.

To fully harness the complementary advantages of multimodal representations, we propose concatenating features from both modalities for multimodal prediction (denoted ‘-

a Microstructure generation examples



b Generation quality assessment

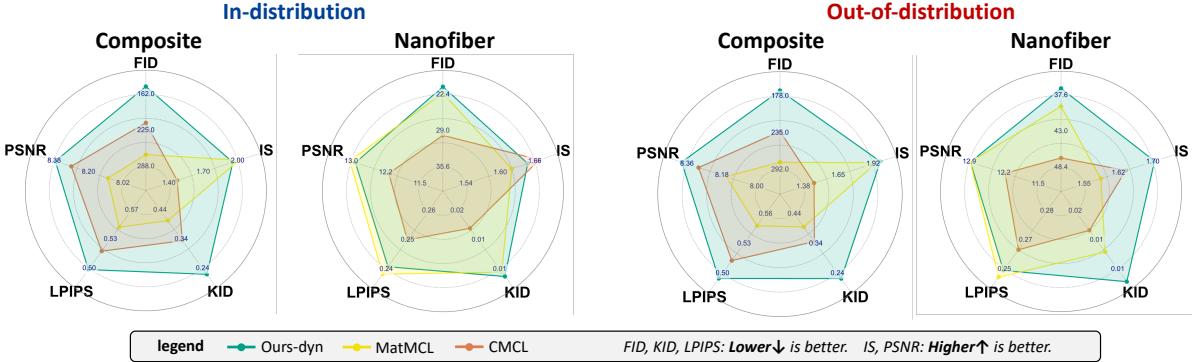


Fig. 4. Descriptor-conditioned microstructure generation. **a** Representative generation examples from ORDER-dyn, CMCL, and MatMCL. Two randomly selected samples are shown for each method. In-distribution samples were observed during prior and decoder training, while out-of-distribution samples are unseen. These examples provide qualitative assessments of pretrained features when assisting the generation of microstructures. **b** Quantitative evaluation of generated samples using five complementary metrics: FID, KID, LPIPS, IS, and PSNR. Outer rings in radar plots indicate better performance. ORDER-dyn achieves consistent improvements compared with multimodal baselines.

fusion'). Figure 3 compares R^2 scores (higher is better) for single-modality and fusion-based predictions. Fusion-based ORDER variants (highlighted with blue borders and shading) consistently outperform all single-modality methods by complementing modality-specific information. Among single-modality approaches, ORDER variants remain optimal across all comparisons. ORDER- α exhibits marginally superior performance compared to ORDER-dyn, though the gap is small and the hyperparameter-free ORDER-dyn still substantially outperforms all other baselines.

The substantial performance gains in both modalities achieved by ORDER stem from its ordinal-aware feature distributions. Intuitively, prediction becomes considerably easier when input features are pre-organized according to target properties, enabling the MLP to exploit continuous property-feature relationships and interpolate between sparsely unobserved samples. This ordinal structure is injected during pretraining via ordinal-aware contrastive learning without compromising cross-modal alignment, as evidenced by ORDER's competitive retrieval accuracy in Figure 2. This dual optimization design distinguishes OR-

DER from existing multimodal frameworks and directly contributes to superior predictive performance.

2.5 Descriptor-conditioned microstructure generation

Image-based generation visualizes the material design process, revealing fiber orientation effects and local microstructures to facilitate defect identification and design optimization. Compared with single tabular modality, image analysis can directly capture more specific spatial fiber distribution. Acquiring high-quality microstructure images generally requires laboring and expensive experiment or simulations. Leveraging ORDER's property-aware multimodal latent space, we can generate realistic microstructures conditioned on input tabular descriptors. Our generation experiments adopt the hyperparameter-free ORDER-dyn to meet practical requirements, since optimal α is hard to obtain in advance when generating unseen structures.

We adopt a two-stage generative framework following DALLE-2 [35]. As illustrated in Figure 1b(iii), the pipeline includes a prior network and a decoder trained on pre-extracted ORDER features. The prior network maps tabular

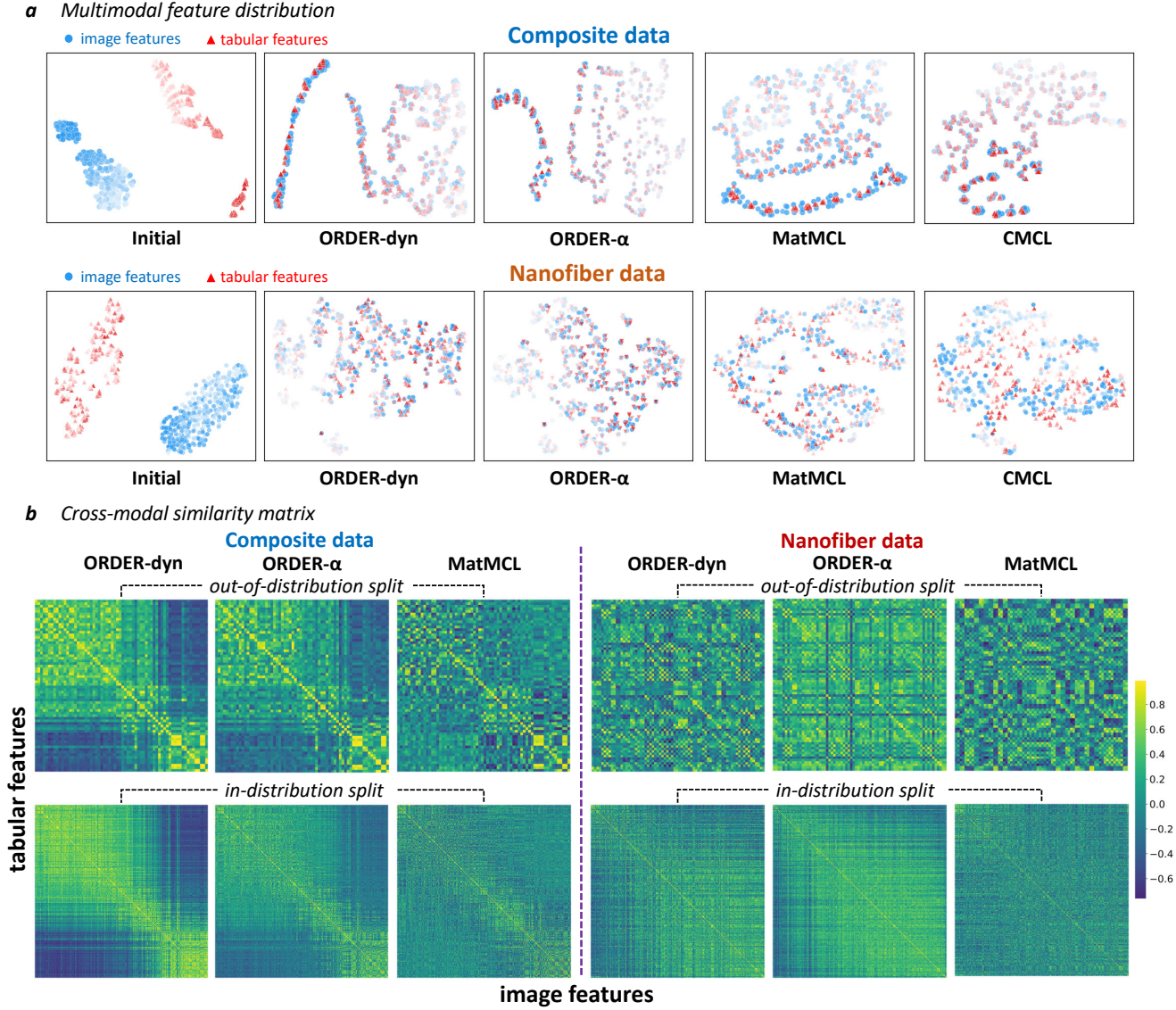


Fig. 5. Visualization of the pretrained multimodal representations using target property ‘Elongation’. **a** The t-SNE projection of multimodal feature space. Darker colors correspond to higher target property values. ‘Initial’ figures show features before pretraining, where image and tabular features distribute apart. After pretraining, ORDER achieves both cross-modal alignment (overlapping distributions) and property-based ordering (color gradients). For Nanofiber data with multiple target properties, features exhibit non-linear low-to-high property trends (left to right). **b** Cross-modal feature similarity matrices for samples sorted by target property values. Brighter color indicates higher similarity and alignment. ORDER exhibits alignment not only between cross-modal pairs, but also with samples with proximate property values.

descriptors to their corresponding image feature distributions, while the decoder synthesizes microstructures from image features using a diffusion-based generative process (detailed in Section 4.4.3). The generative architecture and training procedure remain identical across all compared methods, with only the quality of pretrained multimodal features differs. Therefore, the generation results can directly reflect the representation learning effectiveness.

Figure 4a presents representative generated examples comparing ORDER-dyn with baseline methods on both in-distribution and out-of-distribution samples. On the Nanofiber dataset, ORDER-dyn generates microstructures that reproduce the visual characteristics and fiber density distributions of ground-truth images. In contrast, samples from CMCL and MatMCL exhibit degraded resolution, inconsistent fiber density, and reduced sharpness, indicating substantial distributional gaps relative to real microstructures.

The Composite dataset enables more quantitative assessment of generation quality. Composite microstructures contain circular cross-sections of fibers (corresponding to ‘NumFibre’ in the presented descriptors), represented as cylinders at varying misalignment angles. Fiber colors are rendering artifacts during simulation and do not carry physical meaning. The critical features are fiber count and misalignment consistency. For the in-distribution example with ground truth containing 23 parallel fibers (zero misalignment angle), ORDER-dyn generates samples with 21 and 24 fibers respectively while maintaining zero misalignment angle. The results closely match the target configuration. Conversely, CMCL and MatMCL produce structures with fewer fibers accompanied by spurious shadows, irregular shapes, and misaligned angles. For the out-of-distribution sample containing 21 oriented fibers, ORDER-dyn generates 21 and 20 fibers with appropriate misalignment angles.

Although minor artifacts such as slight blurring and shadows appear, the fiber count remains accurate and overall fidelity is high. CMCL and MatMCL generate fibers with poorly defined boundaries, substantial visual artifacts, and inconsistent morphologies that obscure fiber identification.

Figure 4b provides quantitative evaluation using five different metrics assessing different aspects of generation quality. Fréchet Inception Distance (FID) [36] and Kernel Inception Distance (KID) [37] measure distributional similarity between generated and real images in pretrained Inception feature space. Learned Perceptual Image Patch Similarity (LPIPS) [38] evaluates perceptual similarity using deep neural features. Inception Score (IS) [39] quantifies quality and diversity through predicted class distribution entropy but does not measure alignment with ground truth. Peak Signal-to-Noise Ratio (PSNR) [40] assesses pixel-level reconstruction accuracy. Lower FID, KID, LPIPS and higher IS, PSNR values are preferable.

Radar charts in Figure 4b visualize these metrics for both datasets and distribution regimes, where outer rings represent better performance. ORDER-dyn consistently achieves optimal overall performance across datasets and conditions. On Composite data, ORDER-dyn demonstrates clear improvements across all five metrics. Although MatMCL attains comparable IS scores, its degraded performance on other metrics suggests it generates diverse but structurally inaccurate images that fail to match the ground-truth. For Nanofiber data, MatMCL achieves comparable performance to ORDER-dyn on in-distribution samples but degrades substantially on out-of-distribution data. Performance deteriorates for all methods on unseen properties due to distribution mismatch between data and model, but ORDER-dyn maintains relatively modest degradation, supporting its ability to explore unseen design space based on the ranked features. Note that the metric results on Composite data are worse than Nanofiber results, because the adopted image quality metrics incorporate color information that is meaningless for grayscale Composite microstructures.

These quantitative results support the qualitative observations in Figure 4a. By ensuring that latent features vary continuously with target properties, ORDER produces meaningful and effective priors that interpolate between observed material configurations. Such priors contribute to targeted generation of candidate microstructures with desired characteristics even for unseen design conditions.

2.6 Method analysis

To validate the effects of dual optimization objectives: cross-modal alignment and ordinal awareness, we visualize the multimodal feature spaces learned by our ORDER methods and baseline methods. Figure 5a presents t-SNE [41] visualizations of multimodal features, where darker color indicates larger target property. Before training ('Initial'), image (blue) and tabular (red) features occupy separate regions of the embedding space. Cross-modal contrastive learning encourages modality alignment, and ORDER achieves superior alignment on both datasets, with red and blue points overlapping. In contrast, MatMCL on Composite data and CMCL on Nanofiber data exhibit incomplete alignment with separated modality clusters. Ordinal-aware contrastive

learning further 'sort' the feature space according to target property values. On the simpler Composite dataset, all three methods demonstrate property-correlated distributions, but ours ORDER methods uniquely achieve gradual ordering according to property values. On the more challenging Nanofiber dataset, ORDER features exhibit a small-to-large property trend from left to right, while MatMCL and CMCL show no property-based organization. The multiple target properties in Nanofiber data prevent smooth feature distribution, yet ORDER still forms coherent property-driven structure. These t-SNE visualizations provide intuitive insights that ORDER successfully constructs aligned and property-ordered multimodal space.

Figure 5b presents cross-modal feature similarity matrices with samples **sorted by real target property values**. MatMCL produces sharp diagonal patterns indicating high similarity for matched image-tabular pairs only, which ignores property relationships between similar samples. In addition to strong diagonal signals, ORDER-dyn and ORDER- α also encourage similarities between unmatched samples that decay smoothly with increasing property difference. This structure directly supports the efficacy of ordinal-aware cross-modal property encoding. We can observe that with a constant weighting factor, ORDER- α tend to obtain higher cross-modal similarities (brighter in the similarity matrices) than ORDER-dyn, but the overall similarity trends among the two ORDER variants are similar. On out-of-distribution samples, these patterns weaken but remain observable for Composite data, and ORDER methods continue to exhibit clearer structure than MatMCL on the more challenging Nanofiber dataset. These cross-modal similarity patterns collaborate with the t-SNE analysis to confirm that ORDER effectively constructs aligned and property-ordered multimodal representations. This visualization analysis also provides insights into ORDER's superior downstream performance across retrieval (Figure 2), prediction (Figure 3), and generation (Figure 4) tasks.

3 DISCUSSION

This work focuses on composite materials, whose material structure and properties are decided by fiber distributions in a continuous design space. Therefore, the discrete graph structures widely used to describe crystals and polymers fail to model composite materials. These challenges motivate our design of a vision-tabular pretraining framework for composite material to encode both tabular descriptors and their corresponding microstructural images. Current multimodal pretraining approaches deteriorate for composites with continuous, infinite-dimensional design spaces and extreme data scarcity. To address this, we propose ORDinal-aware image-tabulaR alignment (ORDER) that constructs aligned and property-ordered multimodal representations. ORDER preserves the continuous nature of composite design spaces and interpolates across unobserved design spaces with merely hundreds of data points.

ORDER is evaluated on a public Nanofiber-enforced composite dataset and our in-house CF-T700 Composite dataset. In cross-modal retrieval, ORDER achieves not only competitive accuracy but retrieves candidates with substantially lower property deviation, directly enhancing practical

TABLE 2
Statistical details of the Composite dataset.

	Fiber count	MMA (°)	Vf (%)	Elongation (mm)	Yield strength (MPa)
Minimum	13.0	0.00	0.31	1.6e-4	13.0
Maximum	26.0	4.97	0.65	0.02	2149.8
Average	21.8	1.76	0.48	0.004	488.5

utility for inverse design where multiple viable candidates are needed. ORDER-pretrained features of both modality achieve consistently lower property prediction error than modality-specific models and multimodal baselines. Multimodal fusion of the features bring even better results. The high-quality multimodal representations further help generate microstructures conditioned on tabular descriptors. The generated images exhibit superior fidelity and maintain robust performance on out-of-distribution samples, proving ORDER’s ability to explore unseen design spaces.

Given the scarcity and expense of annotated multimodal composite data, ORDER proposes to adapt pretrained vision-language models through LoRA, a parameter-efficient fine-tuning method. By applying LoRA to CLIP’s vision transformer, ORDER preserves rich pretrained knowledge while injecting domain-specific understanding with merely hundreds of composite material pairs. ORDER can be extended to other scientific domains with continuous properties. Possible future improvements include developing uncertainty quantification methods for predictions and retrieval rankings, and exploring alternative strategies for handling multiple competing target properties.

To conclude, ORDER demonstrates that explicitly modeling property orderliness alongside cross-modal alignment is essential in composite materials. By bridging discrete classification paradigms with continuous regression requirements, ORDER provides a principled framework for integrating heterogeneous composite material data. As foundation models transform scientific discovery, ORDER’s strategy of adapting pretrained knowledge while respecting domain-specific continuous structure offers viable path and insights toward more capable intelligence system for material science.

4 METHODS

4.1 Data preparation

As introduced in Section 2.1, we construct a multimodal Composite dataset based on RVE simulation of CF-T700. Our goal is to comprehensively explore the design space. We achieve this by trying to model as many possible descriptor choices as possible. We only retain descriptors successfully modeled by the Ansys Material Designer, and discard unstable or impractical choices. The resultant dataset includes 436 pairs of descriptors, their corresponding target properties and microstructures. The explored range of descriptor and target property is shown in Table 2. The descriptors include Vf for deciding the number of fiber in the matrix, MMA that decides the rotation angle of fibers and the corresponding orientation tensor. The target properties include tensile yield strength and elongation.

For the obtained microstructures, we center-crop and resize them into size (224,224) to fit the input resolution

of mainstream vision encoders. Random horizontal and vertical flip of probability 0.1 are applied. Since the colors of original images are for display purpose only, we further transform all composite microstructures into grayscale images. All tabular descriptors are unchanged, and treated as continuous input in the table encoder.

We follow the data and preprocessing pipeline in MatMCL [23] for the Nanofiber dataset. The continuous descriptors are standardized using z-score normalization, while discrete descriptors are unchanged.

4.2 Ordinal-aware image-tabular pretraining

The pretraining of ORDER is performed on image and tabular inputs to achieve cross-modal alignment and in-modality orderliness. Recall the notations in Section 2.2. Given original image inputs v_i and tabular inputs t_i , $i \in [1, N]$ where N is the number of sample pairs, the encoders E_t, E_v map them to a shared latent space:

$$h_i^t = E_t(t_i), h_i^v = E_v(v_i), \quad (1)$$

where $h \in \mathbb{R}^d$, $d = 128$ is feature dimension. We propose to optimize the following losses based on the two features.

4.2.1 Cross-modal contrastive loss

The cross-modal contrastive loss was first adopted by Zhang *et al.* [42] to align across modalities, and further proved effective on large scale data by Radford *et al.* [18]. The loss encourages higher similarity between matched cross-modal pairs (positive pairs) and low similarity between other pairs (negative pairs):

$$\mathcal{L}_{v \rightarrow t} = - \sum_i \log \frac{\exp(h_i^v h_i^t / \tau)}{\sum_{j \neq i} \exp(h_i^v h_j^t / \tau) + \exp(h_i^v h_j^v / \tau)}, \quad (2)$$

where τ is temperature parameter and set to 0.1 in this work. We can define $\mathcal{L}_{t \rightarrow v}$ similarly. The overall alignment loss is defined as:

$$\mathcal{L}_{\text{align}} = (\mathcal{L}_{v \rightarrow t} + \mathcal{L}_{t \rightarrow v}) / 2. \quad (3)$$

Note that the alignment loss $\mathcal{L}_{\text{align}}$ has been widely adopted for matching various modalities [19], [21], [23]. Optimization of the loss has become the foundation of multimodal systems.

4.2.2 Ordinal-aware contrastive loss

Inspired by Zha *et al.* [29], we adopt an ordinal-aware contrastive loss on both the image and tabular modality to ensure in-modal feature orderliness with respect to their target properties. The loss encourages higher similarity between feature pairs with more similar target properties, and vice versa. The ordinal-aware contrastive loss for vision features is defined as:

$$\mathcal{L}_v = - \frac{1}{N(N-1)} \sum_i \sum_{j \neq i} \log \frac{\exp(h_i^v h_j^v / \tau)}{\sum_{k \in N, d(i,k) \geq d(i,j)} \exp(h_i^v h_k^v / \tau)}, \quad (4)$$

where $d(i, j)$ computes the target property distance between the i_{th} and j_{th} sample. This work uses L2 distance between normalized target property values for the computation of $d(\cdot)$. The loss \mathcal{L}_t for tabular features can be defined similarly with Eq. (4), and the overall ordinal loss is defined as:

$$\mathcal{L}_{\text{order}} = \mathcal{L}_v + \mathcal{L}_t. \quad (5)$$

The optimization of Eq. (5) encourages the feature space to imitate the distribution of their corresponding target space. While Eq. (5) requires computing target property distances, it does not directly access the target property values. Instead, only the relative order between sample pairs is needed to determine the negative samples. Therefore, there is no need for full target property annotation.

4.3 Model optimization

4.3.1 Preference-guided multi-objective optimization

Our ORDER simultaneously optimizes $\mathcal{L}_{\text{align}}$ and $\mathcal{L}_{\text{order}}$ to obtain an aligned and ordered multimodal feature space. As introduced in Section 4.2, $\mathcal{L}_{\text{align}}$ treats feature pairs from the same modality as negative pairs, while $\mathcal{L}_{\text{order}}$ might push in-modal features with similar target properties closer. Therefore, it is crucial to appropriately handle the optimization of these two conflicting objectives so that the effects of both optimization terms are preserved. We weight the two losses with a hyperparameter $\alpha \in (0, 1)$:

$$\mathcal{L} = \alpha \cdot \mathcal{L}_{\text{order}} + (1 - \alpha) \cdot \mathcal{L}_{\text{align}}. \quad (6)$$

A larger α encourages the model to focus more on in-modal orderliness, while a smaller α leads to more closely aligned cross-modal pairs. One strategy, termed as ORDER- α in this work, selects α with grid-search for each task. ORDER- α achieves better performance, but is time-consuming and might not be realistic in label-scarce scenarios.

To address this, we further propose ORDER-dyn with dynamically adjusted α during optimization. Inspired by Mahapatra *et al.* [24], we adopt a preference-guided strategy to achieve Pareto optimal weighting solutions. Specifically, we formulate the joint optimization of $\mathcal{L}_{\text{align}}$ and $\mathcal{L}_{\text{order}}$ as a multi-objective optimization problem, where we seek parameters that achieve the optimal trade-off between cross-modal alignment and in-modal orderliness.

For simplicity, let $\mathcal{L}_1 = \mathcal{L}_{\text{order}}$ and $\mathcal{L}_2 = \mathcal{L}_{\text{align}}$ denote our two training objectives, with corresponding gradients $g_1 = \nabla_{\theta} \mathcal{L}_1$ and $g_2 = \nabla_{\theta} \mathcal{L}_2$ with respect to model parameters θ . Rather than using a fixed scalar weighting as in Eq. (6), we compute an adaptive update direction h at each training iteration that balances both objectives guided by validation performance. Following preference-guided multi-objective optimization [24], we model the update direction as a convex combination of training gradients: $h = G\beta$, where $\beta = [\beta_1, \beta_2]$ is weight vector with $\beta_1 + \beta_2 = 1$ and $G = [g_1, g_2] \in \mathbb{R}^{n \times 2}$ is the gradient matrix.

To dynamically guide the optimization toward solutions that generalize well to the target domain, we leverage the gradient of $\mathcal{L}_{\text{align}}$ evaluated on a held-out validation set. Specifically, we compute the validation gradient $\hat{g}_v = \nabla_{\theta} \mathcal{L}_{\text{align}}^{\text{val}}$ and use it to steer the optimization direction. The validation set is randomly sampled (15% of the original data) and remains fixed throughout training. We evaluate performance on held-out data because it suggests generalization capability and provides more stable guidance.

The optimal combination $\beta^* = [\beta_1^*, \beta_2^*]^T$ is obtained by solving a linear program that adapts based on the validation loss magnitude. When the validation loss $\mathcal{L}_{\text{align}}^{\text{val}} > \epsilon$ (where

ϵ is a small threshold), we maximize alignment between the update direction and the validation gradient:

$$\begin{aligned} \beta^* &= \arg \max_{\beta \in S_2} (G\beta)^T \hat{g}_v \\ \text{s.t.} \quad &(G\beta)^T g_j \geq \mathbb{1}_{J \neq \emptyset} \cdot \hat{g}_v^T g_j, \quad \forall j \in \bar{J} \setminus J^*, \\ &(G\beta)^T g_j \geq 0, \quad \forall j \in J^*, \end{aligned} \quad (7)$$

where $J = \{j \mid \hat{g}_v^T g_j > 0\}$ identifies objectives whose gradients align with the validation gradient, $\bar{J} = \{1, 2\} \setminus J$, and $J^* = \{j \mid \hat{g}_v^T g_j = \max_{j'} \hat{g}_v^T g_{j'}\}$ identifies the objective most aligned with validation performance. When $\mathcal{L}_{\text{align}}^{\text{val}} \leq \epsilon$, we maximize the sum of gradient projections:

$$\begin{aligned} \beta^* &= \arg \max_{\beta \in S_2} \sum_{j=1}^2 (G\beta)^T \cdot g_j \\ \text{s.t.} \quad &(G\beta)^T \cdot g_j \geq 0, \quad \forall j \in \{1, 2\}. \end{aligned} \quad (8)$$

This formulation ensures that when validation performance is poor ($\mathcal{L}_{\text{align}}^{\text{val}} > \epsilon$), the optimization prioritizes directions that improve validation alignment, potentially allowing controlled ascent on certain training objectives to escape suboptimal regions. Conversely, when validation performance is satisfactory, all training objectives are simultaneously minimized. The indicator function $\mathbb{1}_{J \neq \emptyset}$ equals 1 when at least one training gradient aligns with the validation gradient, and 0 otherwise, preventing unbounded ascent when no training objective benefits validation performance. The parameter update is then $\theta^{t+1} = \theta^t - \eta G\beta^*$, where η is the learning rate. This adaptive strategy allows ORDER-dyn to automatically balance the two objectives without manual hyperparameter tuning, dynamically adjusting the trade-off based on validation feedback to achieve superior generalization performance.

4.3.2 Low-rank adaptation for material-specific knowledge injection

To effectively leverage pretrained knowledge from CLIP while adapting to domain-specific composite materials, we employ Low-Rank Adaptation (LoRA) [27] for parameter-efficient fine-tuning (PEFT) of the vision encoder E_v . LoRA introduces trainable low-rank decomposition matrices into the attention layers of the Vision Transformer, while keeping the original pretrained weights frozen.

The adoption of LoRA addresses two critical challenges in multimodal pretraining for material science. First, paired multimodal material datasets are scarce (typically with merely hundreds of data points) due to expensive characterization procedures. Full fine-tuning of pretrained models like CLIP with these data would lead to severe overfitting and destruction of pre-aligned multimodal structures [43], [44]. LoRA reduces trainable parameters to less than 1% of the original model to substantially mitigate overfitting risks. Second, LoRA preserves the robust visual representations learned from large-scale pretraining on 400M image-text pairs. This enables ORDER to benefit from both general visual understanding and material-specific features without catastrophic forgetting. Our empirical results demonstrate that LoRA-based fine-tuning consistently outperforms training from scratch or using smaller architectures like

ResNet50, validating its effectiveness for multimodal material science applications.

For a pretrained weight matrix $W_0 \in \mathbb{R}^{d \times k}$ in the attention module, LoRA represents the weight update as:

$$W = W_0 + \Delta W = W_0 + BA, \quad (9)$$

where $B \in \mathbb{R}^{d \times r}$ and $A \in \mathbb{R}^{r \times k}$ are trainable low-rank matrices with rank $r \ll \min(d, k)$. With learned matrices A, B , the forward propagation for image input x_i becomes:

$$h_i^v = W_0 x_i + B A x_i. \quad (10)$$

Matrix A is initialized with random Gaussian values, while B is initialized to zero, ensuring $\Delta W = 0$ at the start of training. We apply LoRA to the query, value, key and output projection matrices in all attention layers of the CLIP vision backbone with rank $r = 8$ and scaling factor $\alpha = 16$.

4.3.3 Overall training process

We optimize Eq. (6) with α either pre-defined or decided with multi-objective framework described in Section 4.3.1. The parameters in table encoder E_t are fully fine-tuned. For the vision encoder, we adopt LoRA fine-tuning when using pretrained CLIP, and full fine-tuning for other backbones. In this work, the results for ORDER and CMCL are based on CLIP-pretrained ViT-B/16, and results for MatMCL are based on ImageNet-pretrained ViT-B/16 as MatMCL is not specifically designed for multimodal foundation models.

On all tasks, we pretrain with ORDER and CMCL for 200 epochs under initial learning rate $3e-4$ using Adam optimizer [45]. Batch size is 32 for all methods and tasks. All experiments are implemented with PyTorch [46] and conducted on NVIDIA L40 GPUs.

4.4 Downstream tasks

We first randomly split the data into train (70%), test (15%) and evaluation (15%) sets. The model is first pretrained on train set and applied to the unseen test set for retrieval results. Only ORDER-dyn requires evaluation set during pretraining. The same data splits are used for training prior and decoder models: in-distribution data are from train set and out-of-distribution data are from test set. Following previous work [23], we randomly create a new set of data splits with the same ratio for prediction tasks. The pretrained-then-frozen model is applied to extract multimodal features, and the predictor is trained on features of the train set and predict on the unseen test set. Since our ORDER only requires distance ranking between sample points, such data re-splitting does not cause label leakage. Only the prediction tasks are supervised by target property values.

4.4.1 Cross-modal retrieval

After pretraining, the frozen encoders E_v and E_t produce aligned and ordinal-aware features that enable direct cross-modal retrieval without additional training. For image-to-tabular retrieval, given a query image x_q with extracted feature $h_q^v = E_v(x_q)$, we compute similarities with all tabular features of candidate data split (train split for in-distribution data and test split for out-of-distribution data):

$$s_i = \frac{h_q^v \cdot h_i^t}{\|h_q^v\| \|h_i^t\|}, \quad i \in [1, N], \quad (11)$$

where $h_i^t = E_t(t_i)$ are the precomputed tabular features. The top- k candidates are selected as:

$$\mathcal{R}_k = \{i_1, i_2, \dots, i_k\} \text{ where } s_{i_1} \geq s_{i_2} \geq \dots \geq s_{i_k}. \quad (12)$$

Tabular-to-image retrieval process can be defined similarly. For ORDER- α , we set $\alpha = 0.2$ for Composite data and $\alpha = 0.5$ for Nanofiber data. The ordinal-awareness ensures that retrieved candidates not only match semantically but also exhibit similar target properties, making the retrieval results practically useful for inverse material design.

4.4.2 Target property prediction

We evaluate the quality of learned representations through supervised property prediction tasks. After pretraining, both encoders are frozen and used as feature extractors. A two-layer MLP predictor is trained on the extracted features to predict target properties y_i . For single-modality prediction, the MLP takes either tabular features h_i^t or image features h_i^v as input:

$$\hat{y}_i = f_{\text{MLP}}(h_i^t) \quad \text{or} \quad \hat{y}_i = f_{\text{MLP}}(h_i^v), \quad (13)$$

where f_{MLP} consists of 2 hidden layers of shape (d, d) with ReLU activation, and a final layer of shape $(d, 1)$ that produces prediction results. Note that the target values are normalized using z-score for the training process. We adopt $\alpha = 0.9$ for all prediction tasks with ORDER- α .

For multimodal fusion prediction, we first concatenate features from both modalities and project them to a unified dimension through an additional fusion layer:

$$h_i^{\text{fuse}} = f_{\text{proj}}([h_i^t; h_i^v]) \in \mathbb{R}^d, \quad (14)$$

where $[\cdot; \cdot]$ denotes concatenation and f_{proj} is a linear projection layer of shape $(2d, d)$ that reduces the concatenated feature dimension back to d . The fused representation is then fed into the MLP predictor for prediction as in Eq. (13). This fusion strategy enables the model to leverage complementary information from both modalities that overcomes modality-specific limitations observed in single-modality predictions.

Finally, the predictor and projection for fusion features are optimized with standard mean squared error (MSE) loss:

$$\mathcal{L}_p = \frac{1}{N} \sum_{i=1}^N \|\hat{y}_i - y_i\|^2. \quad (15)$$

For all methods and tasks, we train with learning rate $5e-4$ for 100 epochs using Adam optimizer and batch size 32. Early stopping is applied on Composite dataset to prevent overfitting: if the evaluation loss does not improve for 20 consecutive epochs, the training terminates and the results of the best evaluation epoch are reported.

4.4.3 Descriptor-conditioned microstructure generation

To demonstrate the generative capability of ORDER, we implement descriptor-conditioned microstructure generation following the framework of DALL-E 2 [35]. The generation process consists of two stages: (1) a diffusion prior network that generates image embeddings conditioned on tabular descriptors, and (2) a diffusion decoder network that synthesizes microstructures from these generated embeddings.

Based on pre-extracted features h_i^t and h_i^v , the prior network P is designed to model the conditional distribution $p(h^v|h^t)$. During training, we corrupt the real image feature h_i^v with Gaussian noise at timestep k to obtain $h_{i,k}^v$. The prior network is trained to predict the clean image feature h_i^v given the noisy feature and the tabular condition:

$$\mathcal{L}_{\text{prior}} = \mathbb{E}_{i,k} \|h_i^v - P(h_{i,k}^v, h_i^t, k)\|_2^2, \quad (16)$$

where P outputs the predicted unnoised embedding. At inference, we sample a random Gaussian noise vector and iteratively denoise it using P conditioned on h_i^t to obtain the predicted image feature \hat{h}_i^v .

The decoder network D reconstructs microstructure images conditioned on these image features using a standard Denoising Diffusion Probabilistic Model (DDPM) [47]. We employ D to iteratively predict a noise component ϵ added to the image at timestep k with the following loss function:

$$\mathcal{L}_{\text{decoder}} = \mathbb{E}_{i,\epsilon,k} \|\epsilon - D(v_{i,k}, \hat{h}_i^v, k)\|_2^2, \quad (17)$$

where $v_{i,k}$ is the noised image at timestep k obtained via the forward diffusion process on the ground truth image v_i .

At inference time, given descriptors t_0 of interest, we first extract tabular features: $h_0^t = E_t(t_0)$. We then generate the image feature \hat{h}_0^v via the prior network's reverse diffusion process and finally synthesize the image x_0^{gen} using the decoder D conditioned on \hat{h}_0^v . The target image x_i^{gen} is generated during inference by iteratively denoising from $k = K$ to $k = 0$ using the predicted noise at each step to compute the reverse diffusion update [47], gradually reversing the noise to desired image. For both datasets, the prior and decoder networks are trained for 200 epochs and $\sim 150k$ iterations, respectively, with $K = 1000$ and learning rate $1e-4$ using Adam optimizer. The ordinal structure in the learned feature space ensures that generated microstructures exhibit properties consistent with the input specifications.

5 AUTHOR CONTRIBUTIONS

Xinyao Li designed and implemented the overall method, wrote this manuscript, and conducted experiments on the training, evaluation and analysis of the method. Hangwei Qian participated in the conceptualization of the method, assisted the writing of the manuscript, and led the collection and organization of the Composite dataset. Jingjing Li supervised the project and assisted the writing of the manuscript. Ivor Tsang led this project and participated in the Composite data construction and method conceptualization process. All authors reviewed and approved the final manuscript.

6 COMPETING INTERESTS

The authors declare no competing interests.

7 DATA AVAILABILITY

The Nanofiber dataset is publicly available at <https://github.com/wuyuhui-zju/MatMCL>. Request for our Composite dataset should be addressed to Qian_Hangwei@a-star.edu.sg.

REFERENCES

- [1] E. O. Pyzer-Knapp, J. W. Pitera, P. W. Staar, S. Takeda, T. Laino, D. P. Sanders, J. Sexton, J. R. Smith, and A. Curioni, "Accelerating materials discovery using artificial intelligence, high performance computing and robotics," *npj Computational Materials*, vol. 8, no. 1, p. 84, 2022.
- [2] L. Himanen, A. Geurts, A. S. Foster, and P. Rinke, "Data-driven materials science: status, challenges, and perspectives," *Advanced Science*, vol. 6, no. 21, p. 1900808, 2019.
- [3] G. R. Schleder, A. C. Padilha, C. M. Acosta, M. Costa, and A. Fazzio, "From dft to machine learning: recent approaches to materials science—a review," *Journal of Physics: Materials*, vol. 2, no. 3, p. 032001, 2019.
- [4] R. L. Greenaway and K. E. Jelfs, "Integrating computational and experimental workflows for accelerated organic materials discovery," *Advanced Materials*, vol. 33, no. 11, p. 2004831, 2021.
- [5] A. Talapatra, S. Boluki, P. Honarmandi, A. Solomou, G. Zhao, S. F. Ghoreishi, A. Molkeri, D. Allaire, A. Srivastava, X. Qian *et al.*, "Experiment design frameworks for accelerated discovery of targeted materials across scales," *Frontiers in Materials*, vol. 6, p. 82, 2019.
- [6] J. Wei, X. Chu, X.-Y. Sun, K. Xu, H.-X. Deng, J. Chen, Z. Wei, and M. Lei, "Machine learning in materials science," *InfoMat*, vol. 1, no. 3, pp. 338–358, 2019.
- [7] B. L. DeCost, J. R. Hattrick-Simpers, Z. Trautt, A. G. Kusne, E. Campo, and M. Green, "Scientific ai in materials science: a path to a sustainable and scalable paradigm," *Machine learning: science and technology*, vol. 1, no. 3, p. 033001, 2020.
- [8] M. K. Horton, P. Huck, R. X. Yang, J. M. Munro, S. Dwaraknath, A. M. Ganose, R. S. Kingsbury, M. Wen, J. X. Shen, T. S. Mathis *et al.*, "Accelerated data-driven materials science with the materials project," *Nature Materials*, pp. 1–11, 2025.
- [9] Q. Huang, Y. Li, L. Zhu, Q. Zhao, and W. Yu, "Unified multimodal multidomain polymer representation for property prediction," *npj Computational Materials*, vol. 11, no. 1, p. 153, 2025.
- [10] V. Moro, C. Loh, R. Dangovski, A. Ghorashi, A. Ma, Z. Chen, S. Kim, P. Y. Lu, T. Christensen, and M. Soljačić, "Multimodal foundation models for material property prediction and discovery," *Newton*, vol. 1, no. 1, 2025.
- [11] R. Pollice, G. dos Passos Gomes, M. Aldeghi, R. J. Hickman, M. Krenn, C. Lavigne, M. Lindner-D'Addario, A. Nigam, C. T. Ser, Z. Yao *et al.*, "Data-driven strategies for accelerated materials design," *Accounts of Chemical Research*, vol. 54, no. 4, pp. 849–860, 2021.
- [12] S. T. Khan and S. M. Moosavi, "Connecting metal-organic framework synthesis to applications using multimodal machine learning," *Nature Communications*, vol. 16, no. 1, p. 5642, 2025.
- [13] K. Horie, K. Toda, T. Nakamura, and T. Ideguchi, "Bidirectional quantitative scattering microscopy," *arXiv preprint arXiv:2503.14818*, 2025.
- [14] S. Oh, Y. Jin, S. Lee, W. Li, K. Geauvreau, M. Williams, R. Drake, and A. Bucek, "Taking three-dimensional x-ray diffraction (3dxrd) from the synchrotron to the laboratory scale," *Nature Communications*, vol. 16, no. 1, p. 3964, 2025.
- [15] T. Xie and J. C. Grossman, "Crystal graph convolutional neural networks for an accurate and interpretable prediction of material properties," *Physical review letters*, vol. 120, no. 14, p. 145301, 2018.
- [16] M. Aldeghi and C. W. Coley, "A graph representation of molecular ensembles for polymer property prediction," *Chemical Science*, vol. 13, no. 35, pp. 10486–10498, 2022.
- [17] F. Makni, A.-L. Cristol, M. Kchaou, Y. Desplanques, and R. Elleuch, "Synergistic effects of fibre arrangements on the microstructure and properties of organic composite materials," *Journal of Composite Materials*, vol. 54, no. 29, pp. 4621–4634, 2020.
- [18] A. Radford, J. W. Kim, C. Hallacy, A. Ramesh, G. Goh, S. Agarwal, G. Sastry, A. Askell, P. Mishkin, J. Clark *et al.*, "Learning transferable visual models from natural language supervision," in *International conference on machine learning*. Pmlr, 2021, pp. 8748–8763.
- [19] P. Hager, M. J. Menten, and D. Rueckert, "Best of both worlds: Multimodal contrastive learning with tabular and imaging data," in *Proceedings of the IEEE/CVF Conference on Computer Vision and Pattern Recognition*, 2023, pp. 23924–23935.
- [20] J.-P. Jiang, H.-J. Ye, L. Wang, Y. Yang, Y. Jiang, and D.-C. Zhan, "Tabular insights, visual impacts: transferring expertise from tables to images," in *Forty-first International Conference on Machine Learning*, 2024.

- [21] H. Xu, G. Ghosh, P.-Y. Huang, D. Okhonko, A. Aghajanyan, F. Metze, L. Zettlemoyer, and C. Feichtenhofer, "Videoclip: Contrastive pre-training for zero-shot video-text understanding," *arXiv preprint arXiv:2109.14084*, 2021.
- [22] A. Guzhov, F. Raue, J. Hees, and A. Dengel, "Audioclip: Extending clip to image, text and audio," in *ICASSP 2022-2022 IEEE International Conference on Acoustics, Speech and Signal Processing (ICASSP)*. IEEE, 2022, pp. 976–980.
- [23] Y. Wu, M. Ding, H. He, Q. Wu, S. Jiang, P. Zhang, and J. Ji, "A versatile multimodal learning framework bridging multiscale knowledge for material design," *npj Computational Materials*, vol. 11, no. 1, p. 276, 2025.
- [24] D. Mahapatra and V. Rajan, "Multi-task learning with user preferences: Gradient descent with controlled ascent in pareto optimization," in *International Conference on Machine Learning*. PMLR, 2020, pp. 6597–6607.
- [25] K. He, X. Zhang, S. Ren, and J. Sun, "Deep residual learning for image recognition," in *Proceedings of the IEEE conference on computer vision and pattern recognition*, 2016, pp. 770–778.
- [26] A. Dosovitskiy, "An image is worth 16x16 words: Transformers for image recognition at scale," *arXiv preprint arXiv:2010.11929*, 2020.
- [27] E. J. Hu, Y. Shen, P. Wallis, Z. Allen-Zhu, Y. Li, S. Wang, L. Wang, W. Chen *et al.*, "Lora: Low-rank adaptation of large language models." *ICLR*, vol. 1, no. 2, p. 3, 2022.
- [28] S. Bargmann, B. Klusemann, J. Markmann, J. E. Schnabel, K. Schneider, C. Soyarslan, and J. Wilmers, "Generation of 3d representative volume elements for heterogeneous materials: A review," *Progress in materials science*, vol. 96, pp. 322–384, 2018.
- [29] K. Zha, P. Cao, J. Son, Y. Yang, and D. Katabi, "Rank-n-contrast: learning continuous representations for regression," *Advances in Neural Information Processing Systems*, vol. 36, pp. 17 882–17 903, 2023.
- [30] Y. Gorishniy, I. Rubachev, V. Khruikov, and A. Babenko, "Revisiting deep learning models for tabular data," *Advances in neural information processing systems*, vol. 34, pp. 18 932–18 943, 2021.
- [31] T. Chen, "Xgboost: A scalable tree boosting system," *Cornell University*, 2016.
- [32] N. Hollmann, S. Müller, L. Purucker, A. Krishnakumar, M. Körfer, S. B. Hoo, R. T. Schirrmeister, and F. Hutter, "Accurate predictions on small data with a tabular foundation model," *Nature*, vol. 637, no. 8045, pp. 319–326, 2025.
- [33] L. Prokhorenkova, G. Gusev, A. Vorobev, A. V. Dorogush, and A. Gulin, "Catboost: unbiased boosting with categorical features," *Advances in neural information processing systems*, vol. 31, 2018.
- [34] G. Ke, Q. Meng, T. Finley, T. Wang, W. Chen, W. Ma, Q. Ye, and T.-Y. Liu, "Lightgbm: A highly efficient gradient boosting decision tree," *Advances in neural information processing systems*, vol. 30, 2017.
- [35] A. Ramesh, P. Dhariwal, A. Nichol, C. Chu, and M. Chen, "Hierarchical text-conditional image generation with clip latents," *arXiv preprint arXiv:2204.06125*, vol. 1, no. 2, p. 3, 2022.
- [36] M. Heusel, H. Ramsauer, T. Unterthiner, B. Nessler, and S. Hochreiter, "Gans trained by a two time-scale update rule converge to a local nash equilibrium," *Advances in neural information processing systems*, vol. 30, 2017.
- [37] M. Bińkowski, D. J. Sutherland, M. Arbel, and A. Gretton, "Demystifying mmd gans," in *International Conference on Learning Representations*, 2018.
- [38] R. Zhang, P. Isola, A. A. Efros, E. Shechtman, and O. Wang, "The unreasonable effectiveness of deep features as a perceptual metric," in *Proceedings of the IEEE conference on computer vision and pattern recognition*, 2018, pp. 586–595.
- [39] T. Salimans, I. Goodfellow, W. Zaremba, V. Cheung, A. Radford, and X. Chen, "Improved techniques for training gans," *Advances in neural information processing systems*, vol. 29, 2016.
- [40] Q. Huynh-Thu and M. Ghanbari, "Scope of validity of psnr in image/video quality assessment," *Electronics letters*, vol. 44, no. 13, pp. 800–801, 2008.
- [41] L. v. d. Maaten and G. Hinton, "Visualizing data using t-sne," *Journal of machine learning research*, vol. 9, no. Nov, pp. 2579–2605, 2008.
- [42] Y. Zhang, H. Jiang, Y. Miura, C. D. Manning, and C. P. Langlotz, "Contrastive learning of medical visual representations from paired images and text," in *Machine learning for healthcare conference*. PMLR, 2022, pp. 2–25.
- [43] X. Li, J. Li, Z. Du, L. Zhu, and H. T. Shen, "Unified modality separation: A vision-language framework for unsupervised domain adaptation," *IEEE Transactions on Pattern Analysis and Machine Intelligence*, 2025.
- [44] X. Li, Y. Li, Z. Du, F. Li, K. Lu, and J. Li, "Split to merge: Unifying separated modalities for unsupervised domain adaptation," in *Proceedings of the IEEE/CVF Conference on Computer Vision and Pattern Recognition*, 2024, pp. 23 364–23 374.
- [45] D. P. Kingma, "Adam: A method for stochastic optimization," *arXiv preprint arXiv:1412.6980*, 2014.
- [46] A. Paszke, S. Gross, F. Massa, A. Lerer, J. Bradbury, G. Chanan, T. Killeen, Z. Lin, N. Gimelshein, L. Antiga *et al.*, "Pytorch: An imperative style, high-performance deep learning library," *Advances in neural information processing systems*, vol. 32, 2019.
- [47] J. Ho, A. Jain, and P. Abbeel, "Denoising diffusion probabilistic models," *Advances in neural information processing systems*, vol. 33, pp. 6840–6851, 2020.